Adsorption of Cu (II) onto Bamboo Supported Manganese (BS-Mn) Nanocomposite: Effect of Operational Parameters, Kinetic, Isotherms, and Thermodynamic Studies

ADEWUMI O DADA[1*], DAYO F LATONA[2], OLUSEGUN J OJEDIRAN[3], OSAZUWA O. NATH[1]

[1*]*Department of Physical Sciences, Industrial Chemistry, Landmark University, P.M.B.1001, Omu-Aran, Nigeria*
[2]*Department of Chemical Sciences, Osun State University, Osogbo, Nigeria.*
[3]*Department of Agricultural and Bio-system, Landmark University, P.M.B.1001, Omu-Aran, Nigeria*
**Corresponding author's e-mail: *dada.oluwasogo@lmu.edu.ng or dada.oluwasogo@landmarkuniversity.edu.ng*

ABSTRACT: Bamboo supported manganese (BS-Mn) nanocomposite was prepared in a single pot system via bottom-up approach using a chemical reduction method. Langmuir surface area, BET surface area, and Single pore surface area were 349.70 m^2/g, 218.90 m^2/g, and 213.50 m^2/g, respectively. The pore size (24.34 Å); pore volume (0.489 cm^3); point of zero charge (5.8); bulk density (0.0035 gcm^{-3}); specific surface area (33.00 m^2/g) by Saer's method and functional group of BS-Mn nanocomposite determined using Fourier Transform Infrared Spectrophotometer (FTIR). Various operational parameters affecting adsorption of Cu(II) such as adsorbent dose (100 mg), pH (6), contact time (90 min), initial Cu(II) ions concentration (100 mg/L) and temperature (298 K) were determined in a batch technique. Kinetic data were best fitted to pseudo second-order model validated by sum of square error (SSE) and Chi-square test (χ^2). Equilibrium data were better described by Langmuir isotherm model with the monolayer adsorption capacity surpassing those previously reported for Cu(II) uptake. The thermodynamic parameters, ΔG^o (-31.773 kJ mol^{-1}), ΔS^o (107.30 J) and ΔH^o (+202 kJmol^{-1}) revealed that the adsorption process was feasible, spontaneous and endothermic in nature. The study showed that BS–Mn is a promising nanocomposite which could be utilized for industrial wastewater remediation. @JASEM

Keyword: BS-Mn Nanocomposite; Copper; Adsorption; Kinetics; Isotherms; Spontaneous

Nomenclature
C_o = Initial concentration of the Cu^{2+} before adsorption (mg L^{-1});
C_e = equilibrium concentration of the Cu^{2+} solution (mg L^{-1});
W = Dry weight in gram of the nano-adsorbent;
V = Volume of the Cu^{2+} solution (mL);
q_e = Amount of Cu^{2+} adsorbed at equilibrium per unit weight of the adsorbent (BS-Mn) (mg g^{-1});
q_t = Amount of Cu^{2+} adsorbed at any time (mg/g);
k_1 = Pseudo first-order rate constant (min^{-1});
k_2 = rate constant of pseudo second-order adsorption (g/mg min);
h_1= Pseudo first-order initial adsorption rate (mg/g.min);
h_2 = Pseudo second-order initial adsorption rate (mg^2/g^2min);
α = Constant of the Elovich rate equation (g min^2/mg);
β = Constant in the Elovich rate equation (g min/mg);
k = Fractional power rate constant;
R = Gas constant (J/mol K);
K_f = Freundlich isotherm constant;
n_f = exponent in Freundlich isotherm;
Q_{max} =Maximum monolayer coverage capacity(mg.g^{-1});
K_L = Langmuir isotherm constant (L.mg^{-1});
R_L = Dimensionless constant referred to as separation factor;
R^2 = Coefficient of Correlation or Regression Coefficient
b_T = Temkin isotherm constant related to the heat of adsorption;
A_T = Temkin isotherm equilibrium binding constant (Lg^{-1});

A_{DKR} = DKR isotherm constant (mol^2/kJ^2) related to free adsorption energy;
q_d = Theoretical isotherm saturation capacity (mg/g);
$\mathcal{E}$ = Polanyi potential = RT ln(1 + 1/C_e)
E = Mean adsorption free energy,
θ = Degree of surface coverage
k_{id} = Intraparticle diffusion rate constant (mg.$g^{-1}min^{0.5}$)
C = Thickness of the boundary.
R^2 = Regression coefficient,
ΔH^o = Standard enthalpy change (kJ mol^{-1});
ΔS^o = Standard entropy change (J $mol^{-1}K^{-1}$);
ΔG^o = Standard Gibbs free energy (kJ mol^{-1}),
T = Absolute Temperature (K)
K_c = Thermodynamic equilibrium constant

Nanotechnology offers the potential of creating material and device which take advantage of unique phenomena realized at such scale length (Dhermendra *et al.,* 2008). It is finding more relevance in environmental remediation especially in the removal of toxic heavy metal ions as a result of effective and efficient adsorbents utilized. Copper as the heavy metal investigated in this research gets into the environment via several means (both anthropogenic and natural process), causing pollution to water bodies, soil and the atmosphere at large (Dada *et al.,* 2015a; Jun and Nancy, 2000). Chemical industries, metallurgy, metal smelting, copper mining, electronic and electrical industries are other sources of copper in the environment (Kordosky *et al.,* 2002).

Copper ions have been listed as one of the potential threat to human beings; aquatic organisms and plants. Main exposure of human to copper occurs primarily

**Corresponding author's e-mail: *dada.oluwasogo@lmu.edu.ng*

from the consumption of drinking water due to copper plumbing (Fawell, 2004), about 20 to 25% of copper intake comes from drinking water (Michael *et al.,* 2001). The oxidative potential of copper may be responsible for some of it toxicity, it produces oxidative damage to biological system including peroxidation of lipid or other macromolecules (Nuran *et al.,* 2000). Other precarious effect of copper are excessive excretion, anorexia, disorderliness, reduction in the rate of photosynthesis, *cirrhosis, necrosis*, headaches, stomachaches, dizziness, hematemesis, diarrhea, hypotension, melena, coma, jaundice, cirrhosis, gastrointestinal distress and fatal mortality rate, gastric hemorrhage, tarchy cardia, hypotension, hemolytic crisis, convulsion and paralysis (Dada *et al.,* 2015b; Bonnie *et al.,* 2007). The main target organs of copper ions are liver, kidney and brain adversely affecting central nervous system and lower the immune system which can eventually lead to death of the affected organism.

Effort has been made on the removal of heavy metal ions using different methods such as chemical precipitation, membrane process, ion exchange, solvent extraction, electrodialysis and reverse osmosis but they suffer several disadvantages such as high cost of operation, incomplete metal ion removal, high reagent and energy consumption, generation of toxic sludge and other waste products that require disposal or treatment (Prasad and Elumalai, 2011; Dada *et al.,* 2012; Dada *et al.,* 2013). However, adsorption has been identified as an attractive alternative, unique, effective, efficient and low cost method of removing heavy metal ions from the environment (Adekola *et al.,* 2012; Dada *et al.,* 2014).

Raw bamboo has been extensively used as efficient precursor in the preparation of activated carbon due to its moderately high carbon content (48.64%) and low amounts of nitrogen (0.14%), sulphur (0.11%) and hydrogen (6.75%) (Edward *et al.,* 2008). In recent years, raw and activated bamboo have been recognized and utilized as promising adsorbent for adsorption of heavy metal ions (Hsu *et al.,* 2009; Lo *et al.,* 2012; Zhao *et al.,* 2012). However, the use of bamboo as a precursor in preparing nanocomposite has not been reported by any researcher, hence the focus of this study. In this study, bamboo was used as one of the precursors, serving as a base material in the preparation of bamboo supported manganese nanocomposite.

MATERIALS AND METHODS
Chemicals materials used: All through this work, analytical grade reagents were used. Sodium borohydride (NaBH₄) (Qualikems, India), CuSO₄.5H₂O (Breckland Scientific, UK), Manganese Chloride, Isopropyl alcohol (BDH), were used. Vacuum filtration

setup, 0.45 μm milipore filter paper, Laboratory test sieve (Ende Cotts, tolerance full, Pat No. 66924, Bs 410, Ser. No. 153878, Aperture 250 μm, and Ser.No. 220460, Aperture 150 μm).

Preparation of Bamboo Supported Manganese (BS–Mn) Nanocomposite: The bamboo supported manganese (BS-Mn) nanocomposite was prepared following the procedure earlier reported by Dada *et al.,* (2015a). The bamboo used as base material in this research was collected around the construction site in the vicinity of Landmark University campus, Nigeria. Physicochemical parameters such as Langmuir, BET and specific surface area, pore size, pore volume, bulk density and point of zero charge were determined. The functional group on BS-Mn was determined using Fourier Transform Infrared Spectrometer.

BET, Bulk density, Point of Zero Charge and FTIR Characterization of BS-Mn: The analysis on the determination of surface area. pore size and volume were performed following Brunauer-Emmett-Teller (BET) and Barrett-Joyner-Halenda (BJH) methods using Micrometritics AutoChem II Chemisorption Analyzer. The bulk density was determined using Archimedes' principle, the Point of Zero charge (PZC) was determined using a procedure elsewhere in literature (Srivastava *et al*., 2006). The pH was varied from 2 to 12 by adjustments with 0.1 M HNO₃ and 0.1 M NaOH. The functional groups on BS-Mn were also determined using Schimadzu FTIR model IR 8400S

Preparation of Adsorbate: Carefully weighed 3.39 g of CuSO₄ was dissolved in 1000 mL of distilled deionized water for the preparation of 1000 ppm Cu^{2+} stock solution. Working concentrations of 20, 40, 60, 80, and 100 ppm were prepared by serial dilution for the adsorption studies.

*Adsorption Experiment***:** Adsorption studies were carried out using batch techniques following the procedure reported by [12]. In a typical experiment, 0.1 g of BS-Mn was introduced into 50 mL of 60 mL Teflon bottle, agitated intermittently on the orbital shaker for 3 h at various optimum operational factors. Residual concentration was immediately determined using atomic adsorption spectrophotometer (AAS) model AA320N. This was done in triplicate and the mean value for each set of the experiments was used. Adsorption capacity and the removal efficiency were obtained using Eqs. 2 and 3 respectively (Hameed *et al.,* 2008):

$$Q_e = \frac{(C_o - C_e)V}{W} \tag{1}$$

ADEWUMI O DADA[1]*, DAYO F LATONA[2], OLUSEGUN J OJEDIRAN[3], OSAZUWA O. NATH [1]

$$\% \ RE = \frac{C_o - C_e}{C_o} \times 100 \qquad (2)$$

Effect of adsorption on various initial concentrations from 20 – 100 mgL^{-1} were thereafter studied. Equilibrium data obtained analyze using isotherm models. Other operational factors such as the effect of adsorbent dose, effects of pH, contact time, and temperature were carried out following a similar procedure (Adekola *et al.,* 2012; Hao *et al.,* 2010). Effect of contact time on the uptake of Cu^{2+} was investigated by varying the time of adsorption from 10, 30, 60, 90, 120 minutes at optimum conditions. Effect of pH was studied at by varying the pH of the solution from 2 to 12 using 0.1 M NaOH and 0.1 M HNO$_3$ solutions as appropriate. Effect of adsorbent dose was studied by varying quantities of the BS–Mn (10, 40, 60, 80 and 100) mg at optimum conditions (Dada *et al.,* 2015b).

*Batch Kinetic Experiment***:** Batch kinetics studies was carried out on the removal of copper (II) ion from aqueous solutions. The aqueous samples were taken at different time intervals (10, 30, 60, 90 and 120 mins), and then the concentration of copper (II) ion were determined using AAS. The amount adsorbed at time *t*, q_t (mgg^{-1}), was calculated using Eq. 3 (Dada *et al.,* 2015a; Dada *et al.,* 2015b; Hao *et al.,* 2010):

$$q_t = \frac{(c_o - c_t)V}{W} \qquad (3)$$

Where C_o, C_t, q_t, *V and W* are well defined earlier in the nomenclature. The data obtained were analyzed using pseudo first-order, pseudo second-order, Elovich and fractional power. Mechanism of the system was determined using intraparticle or pore diffusion, liquid film or surface diffusion, Bangham and Boyd models.

*Effect of Temperature***:** The temperature was varied while maintaining constant other physico-chemical parameters (concentration, adsorbent dose, time and pH). 0.1 g of BS-Mn nanocomposite was contacted with Cu^{2+} solution at the equilibrium concentration at pH 5.5 while varying the temperature from 298 K – 338 K.

RESULTS AND DISCUSSION
Characterization: The physicochemical properties of bamboo supported managanese (BS-Mn) nanocomposite was determined vis-à-vis point of zero charge, bulk density, surface area, pore volume, and pore size. The surface physical properties of the BS-Mn nanocomposite was characterized with a Micromeritics ASAP 2020, using N$_2$ at 77 K. The single pore surface area 213.5 m^2/g, BET surface area 218.9 m^2/g and Langmuir surface area 349.7 m^2/g together with other properties obtained as shown in Table 1 revealed the suitability of BS-Mn nanocomposite for adsorption of Cu^{2+} as a result large pores (Dada *et al.,* 2015a)

Table 1: Physicochemical properties of BS-Mn nanocomposite

Physicochemical Parameters	Adsorbent (BS–Mn nanocomposite)
Point of Zero Charge (PZC)	5.8
Bulk Density (g/cm^3)	0.0035
Specific Surface Area by Sear's Method S(m^2/g) = 32-25	33
SURFACE AREA	
(a) Single pore surface area m^2/g	213.4706
(b) BET surface area m^2/g	218.8812
(c) Langmuir surface area m^2/g	349.686
(d) BJH adsorption cumulative surface area of pore m^2/g	253.7744
(e) BJH desorption cumulative surface area of pore m^2/g	186.352
PORE VOLUME	
(a) single point adsorption total pore volume pores cm^3/l	0.489585
(b) single point desorption total pore volume pores cm^3/l	0.49259
(c) BJH adsorption cumulative volume of pores cm^3/l	0.505618
(d) BJH desorption cumulative volume of pores cm^3/l	0.512784
PORE SIZE	
(a) adsorption average pore width (Å)	24.344
(b) desorption average pore width (Å)	24.5631
(c) BJH adsorption pore width (Å)	37.973

The prominent vibrational bands are shown in the FTIR Spectrum of BS-Mn nanocomposite presented in Fig. 1. The functional groups and their corresponding bands are: O-H (3417 cm^{-1}), C-H stretching (2362 cm^{-1}), H-O-H (1301 cm^{-1}), Cl– (977 cm^{-1}), Mn^o (570 cm^{-1}). These functional groups also participated in the adsorption studies supporting a chemisorption mechanism (Dada *et al.,* 2015b).

ADEWUMI O DADA[1]*, DAYO F LATONA[2], OLUSEGUN J OJEDIRAN[3], OSAZUWA O. NATH [1]
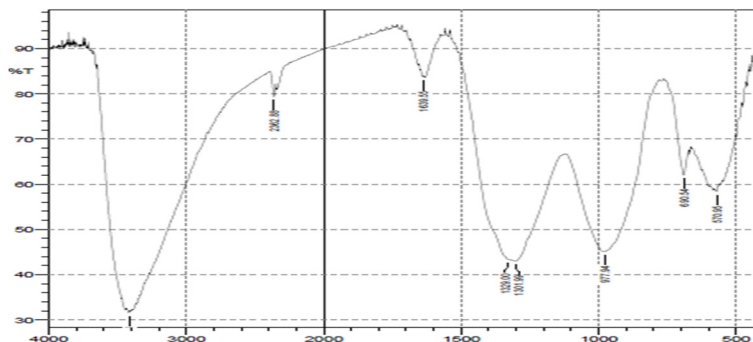
Fig 1: FTIR Spectrum of Bamboo supported Manganese (BS-Mn) Nanocomposite

Effects of Adsorbent dose, pH, Contact time and Initial Concentration: Effect of adsorbent dose in needed in order to maximize the interaction between the Cu^{2+} and BS-Mn nanocomposite. Analysis of this plot (Fig. 2) showed that percentage of Cu^{2+} removed increased with an increase in the adsorbent dose from 65.6% to 100 % as a result of increase in the number of active binding exchangeable sites and large surface areas until equilibrium was achieved (Fu-Lan *et al.*, 2009; Mohammed *et al.*, 2012).
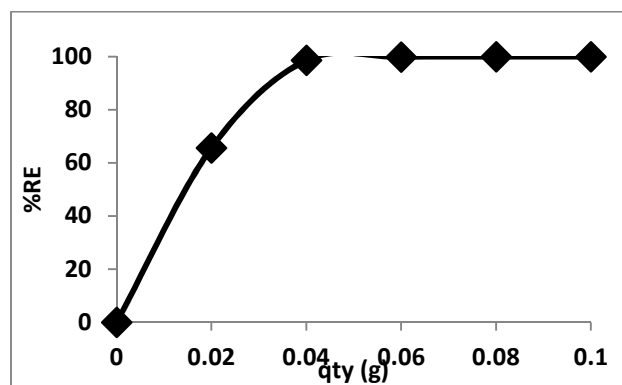
more implicit from the knowledge of the point of zero charge (PZC). Adsorption of anionic hazardous species proceeds at pH higher than $pH_{(PZC)}$, while at pH lower than $pH_{(PZC)}$, adsorption of cationic specie proceeded. This is the major reason why there was an increase in the adsorption of Cu^{2+} at higher pH values between pH 5 – 7 (Fig 3).
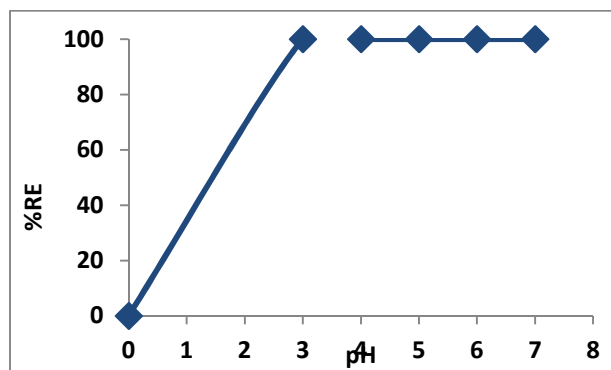

Fig 3: The effect of pH on Cu^{2+} adsorbed onto BS–Mn nanocomposite

Fig. 2: Effect of BS-Mn nanocomposite dose on Cu^{2+} adsorbed

Optimum adsorbent dose obtained was 100 mg which was used for the subsequent studies.

From the study of effect of pH on the adsorption of Cu^{2+} onto BS-Mn nanocomposite system, low removal efficiency observed at lower pH could be attributed to the fact that at low pH_i (pH 3) the surface of the adsorbent acquired anionic charge, the high H^+ compete with Cu^{2+} in the solution, thus decreasing adsorption capacity of Cu^{2+}. Therefore, protonation and cationic competition for the available adsorption site led to this decrease. At high pH (5 – 6) the surface of the adsorbent have a net positive charge, decrease in H^+ concentration (deprotonation) in the solution favored the adsorption of Cu^{2+} thereby leading to increase in the removal efficiency as observed in Fig 3. This phenomenon can be

The graph of percentage adsorbed of copper (II) ion against contact time as represented in Fig. 4 revealed that the percentage adsorption of Cu^{2+} was rapid at the initial stage and then became relatively slow with maximum percentage of 99.9% of Cu^{2+} adsorbed at 90 minutes. This is due to the fact that large number of vacant sites were available for adsorption during the initial stage, as the number of vacant site decreases, adsorption rate become slow due to probably the slow pore diffusion of Cu^{2+} on the adsorbent and repulsive force between the solid molecules and the bulk phase. This finding is similar to the report of Xiao *et al.*, (2011). The initial concentration on adsorption of Cu^{2+} onto BS-Mn plays a key role as a driving force to overcome the mass transfer resistance between the Cu^{2+} solution and BS-Mn. The removal efficiency increases with increase in Cu^{2+} from 20 to 100 mgL^{-1} as result of availability of adsorption sites until equilibrium was reached when the sorption

ADEWUMI O DADA[1]*, DAYO F LATONA[2], OLUSEGUN J OJEDIRAN[3], OSAZUWA O. NATH [1]

sites have been saturated with Cu^{2+} (Fig. 5). Advantageously, 99.5% of Cu^{2+} was removed even at higher Cu^{2+} concentration as a result of increase in driving force due to the concentration gradient developed between the bulk solution and surface of the adsorbents. This result was similar to what was reported by Dada *et al.,* (2013) and Aluigi *et al.,* (2014).
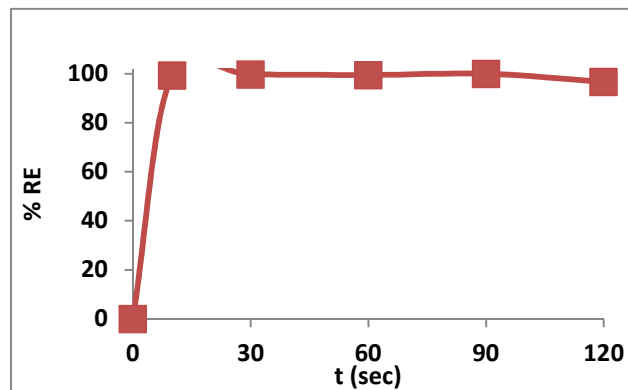

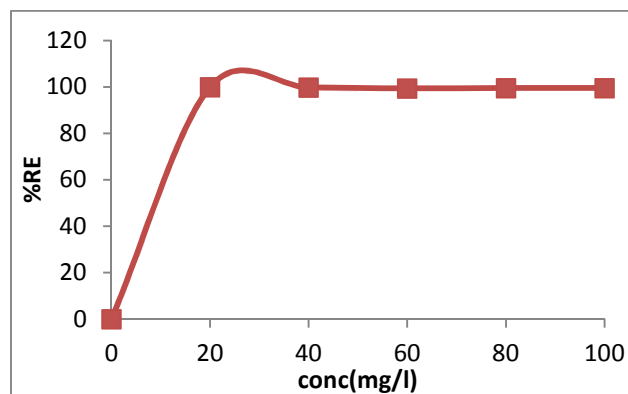Fig 4: The effect of Contact time on Cu^{2+} adsorbed onto BS–Mn

Fig 5: The effect of Initial Concentration on Cu^{2+} adsorbed onto BS–Mn

Adsorption Kinetics on uptake of Cu^{2+} onto BS-Mn Nanocomposite system: The kinetics of adsorption of Cu^{2+} was investigated in order to determine the rate of mechanism of the adsorption process. Four kinetic models namely; Pseudo first-order, Pseudo second-order, Elovich and Fractional power rate equations were us to describe and analyze the experimental data. The evaluated parameters presented in Table 2 were obtained from linear plots in Figs. 6 (a – d)

Lagergren Pseudo First-order kinetics: The pseudo first-order equation (Lagergren's equation) describes adsorption in solid–liquid systems based on the adsorption capacity of solids (Ho 2004). This model

works on the assumption that one Cu^{2+} ion is sorbed on one site of adsorption on the BS-Mn nanocomposite surface as described by the Eq.4:

$$S + Cu^{2+}_{aq} \xrightarrow{k_2} S.Cu_{solid\ phase} \qquad (4)$$
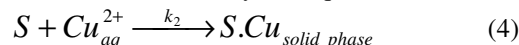
Where S is an unloaded adsorbent (BS-Mn nanocomposite) which is unoccupied sorption site. The linear equation of pseudo first-order is given as:

$$Log(q_e - q_t) = Log\ q_e - \frac{k_1 t}{2.303} \qquad (5)$$

$$h_1 = k_1 q_e \qquad (6)$$

Where h_1 is the initial adsorption rate from pseudo first-order rate equation, the plot of $log(q_e - q_t)$ versus t gave a linear relationship (Fig 8a). However, the evaluated parameters k_1 and q_e calculated were determined from the slope and intercept of the plot of the best fit line (Table 2). Based on the low correlation coefficient R^2 and disparity between the q_e, experimental and q_e, calculated, the adsorption of Cu^{2+} onto BS-Mn was poorly described by pseudo first-order.

Pseudo Second-order Kinetics model: The pseudo second-order kinetic model has been applied for analyzing chemisorption kinetics from liquid solutions (Azizian 2004). This model assumes that one copper ion is sorbed onto two sorption sites on BS-Mn nanocomposites' surface according to the Eq 7:

$$2S + Cu^{2+}_{aq} \xrightarrow{k_2} S_2 Cu_{solid\ phase} \qquad (7)$$
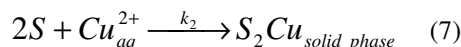
The pseudo second-order linear expression is given as:

$$\frac{t}{q_t} = \frac{1}{h_2} + \frac{1}{q_e} t \qquad (8)$$

$$h_2 = k_2 q_e^2 \qquad (9)$$

Where q_t, q_e, h_2 and k_2 parameters have been well defined in the nomenclature. Both h_2 and k_2 were determined from the slope and intercept of the linear plot of t/q_t against t (Fig. 8b). From the evaluated parameters presented in Table 2, the closeness and good agreement between the q_e, experimental (20 mg g^{-1}) and q_e calculated (19.985 mg g^{-1}) coupled with the regression coefficient (R^2= 1) and high value of pseudo second-order initial adsorption rate (h_2 = 72.9927 mgg^{-1}min^{-1}) confirmed that pseudo second-order is best in describing the adsorption of Cu^{2+} onto BS-Mn

Elovich Model: The Elovich equation is expressed as:

$$q_t = \frac{1}{\beta} \ell n(\alpha\beta) + \frac{1}{\beta} \ell n(t) \qquad (10)$$

ADEWUMI O DADA[1]*, DAYO F LATONA[2], OLUSEGUN J OJEDIRAN[3], OSAZUWA O. NATH [1]

where q_t is the amount of adsorbate per unit mass of sorbent at time (t), $\propto$ is the initial adsorption rate (mg/g-min); β is the desorption constant (g/mg) during any one experiment (Ahmad *et al.,* 2014a; Song *et al.,* 2014; Igwe and Abia, 2006). Both α and β were determined from the slope and intercept of the plot of q_t versus ln(t) (Fig 8c). Based on the evaluated parameters in Table 2, the Elovich model also described the adsorption kinetic of adsorption of Cu^{2+} onto BS-Mn. It can be inferred that 1/β value (0.2019) reflects the number of sites remaining after adsorption whereas the value of *1/βln(αβ)* (19.065) indicates the adsorption quantity when ln(t) equals to zero. The closeness of the value of *1/βln(αβ)* to experimental quantity adsorbed revealed the fitting of the kinetic data to Elovich model.

Factional Power: The fractional power model also known as Power Function can be expressed linearly as:

$$\ell og\ (q_t) = \log(k) + v \log(t) \tag{11}$$

Where all parameters remain as early defined in the nomenclature. The parameters v and k were determined from slope and intercept of a linear plot of log (q_t) versus log (t) (Ayanda *et al.,* 2013). From the evaluated parameters presented in Table 2, the value of v being positive and less than unity coupled with the close agreement between q_e experimental and q_e, calculated

are indications of the best fitting of the kinetic data to fractional power model.

*Validity of Adsorption Kinetic Models***:** The suitability, agreement and best fit among the kinetic models were judged using the statistical tools such as regression coefficient (R^2), sum of square error (SSE) and Chi-square test (χ^2). The established mathematical expressions of SSE and χ^2 are given in Eq 12 and 13 (Foo and Hameed, 2010):

$$SSE = \sum_{i=1}^{n} \left(q_{e,cal} - q_{e,\exp}\right)^2 \tag{12}$$

$$\chi^2 = \sum_{i=1}^{n} \frac{\left(q_{e,\exp} - q_{e,cal}\right)^2}{q_{e,cal}} \tag{13}$$

The closer the regression coefficient (R^2) to unity coupled with good agreement between the experimental and the calculated quantity adsorbed (q_e, exp and q_e, cal respectively) and lower values of SSE and χ^2, the better the kinetic model in describing the data. Magnitude of both sum of square error (SSE) and non-linear chi-square test (χ^2) depends on the agreement between the q_e, experimental and the q_e, calculated (Boparai *et al.,* 2011). Based on the evaluated parameter in Table 2, it can therefore be judged that Pseudo second-order model is best in describing the kinetic data.
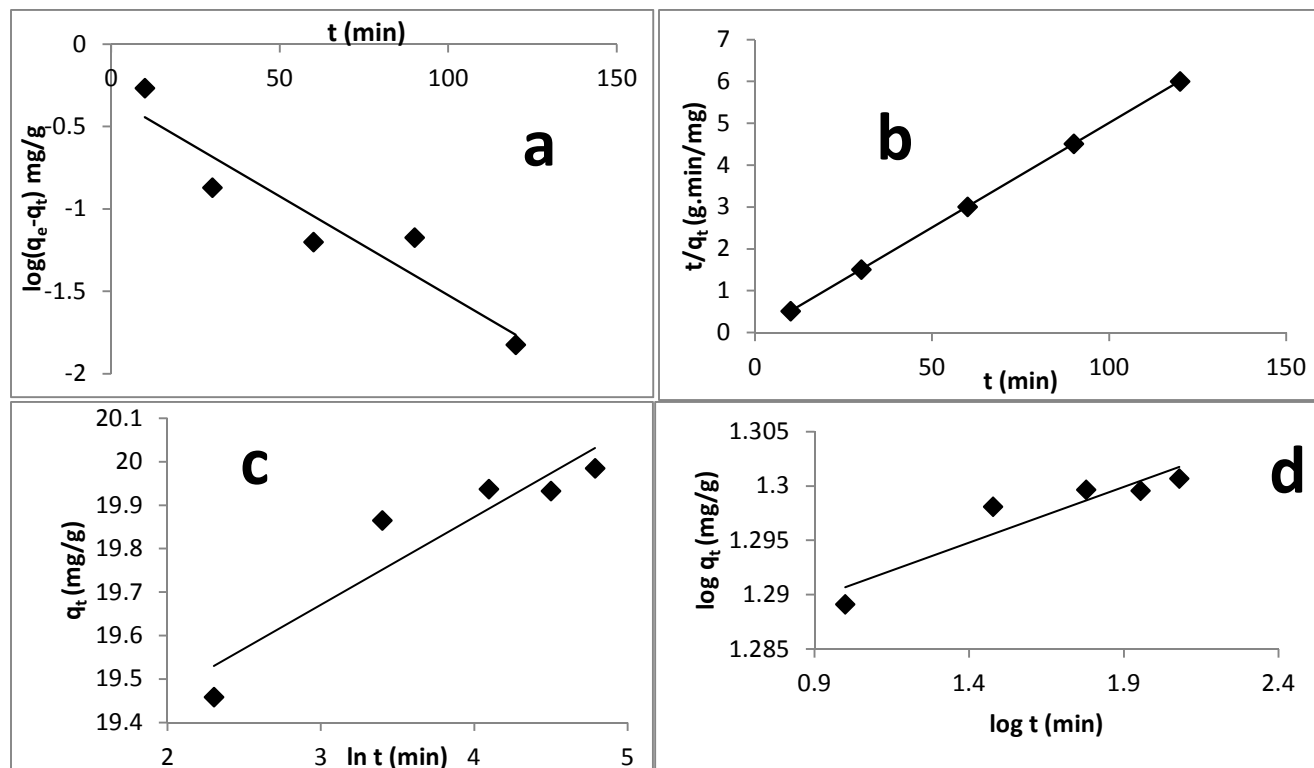

Fig 6: Linearized plots of (a) Pseudo first order (b) Pseudo second-order (c) Elovich (d) Fractional power kinetic models

ADEWUMI O DADA[1]*, DAYO F LATONA[2], OLUSEGUN J OJEDIRAN[3], OSAZUWA O. NATH [1]

Adsorption Mechanisms: Determination of the adsorption rate controlling step enhances understanding of the adsorption mechanism. In order to determine this, the kinetic data were analyzed using intraparticle or pore diffusion, liquid film or surface diffusion, Bangham and Boyd models (Fig. 7(a – d). Two general models used to describe the sorption rate are: Intraparticle or pore diffusion and liquid film diffusion models. Weber Morris Intraparticle diffusion model involves pore diffusion where adsorbate molecules percolate into the interior of adsorbent particles. Its mathematical expression is given as (Weber and Morris, 1963):

$$q_t = k_{id}t^{0.5} + C \qquad (14)$$

where k_{id} is the intraparticle diffusion rate constant and C is the intercept determined from the plot of q_t versus $t^{0.5}$ (Igwe *et al.,* 2008; Chingombe *et al.,* 2006) which were both determined from the slope and intercept of the linear plot. From Fig. 7a, and evaluated parameters in Table 3, the value of $k_{id} = 5.96$ x10^{-2} $mgg^{-1}min^{-0.5}$ and the value of C = 19.397 which indicates the thickness of the adsorbents and a reflection of the boundary layer effect suggesting a larger contribution of the surface to the rate determining step (Ahmad *et al.,* 2014a). However, since the plot of q_t versus $t^{0.5}$ did not pass through the origin thus intraparticle diffusion was not the sole rate determining step (Ozcan *et al.,* 2007; Taqui *et al.,* 2007; Wu *et al.,* 2009).

Table 2: Adsorption Kinetic models' parameters for the sorption of Cu^{2+} onto BS-Mn nanocomposite

Pseudo first-order	parameters	Pseudo Second-order	parameters	Elovich	parameters	Fractional Power	parameters
q_e,exp (mg/g)	20.00	q_e, exp (mg/g)	20.00	q_o,exp (mg/g)	20.00	q_e,exp (mg/g)	20.00
q_e, cal (mg/g)	0.4752	q_e, cal (mg/g)	19.985	q_e, cal (mg/g)	19.9735	q_e, cal (mg/g)	19.9725
$k_1(min^{-1})$	2.76x10^{-2}	$k_2(g/mg/min)$	1.824x10^{-1}	$\alpha(g.min^2/mg)$	2.06x10^{40}	$v(min^{-1})$	0.0102
h_1 (mg/g/min)	1.31x10^{-2}	h_2 (mg/g/min)	72.9927	$\beta(g.min/mg)$	4.9529	k_3 (mg/g)	19.0765
R^2	0.8853	R^2	1	R^2	0.8716	$k_3v(mg/g/min)$	0.1945
SSE	380.6284	SSE	2.25x10^{-4}	SSE	1.323x10^{-4}	R^2	0.8703
χ^2	800.9857	χ^2	1.125x10^{-5}	χ^2	6.62x10^{-6}	SSE	7.56x10^{-4}
						χ^2	3.78x10^{-5}

Liquid film also known as surface diffusion is another adsorption mechanism where the adsorbate is transported from the bulk solution to the external surface of adsorbent. The liquid film diffusion is expressed by the Eq. 15 given below (Igwe and Abia 2006; Ayanda *et al.,* 2013; Igwe *et al.,* 2015):

$$\ln(1 - F) = -k_P t \qquad (15)$$

$$\text{Where } F = \frac{[q]_t^n}{[q]_e^n} \qquad (16)$$

F is fractional attainment to equilibrium, k_p is the rate coefficient for particle-diffusion controlled process corresponding to the particle size of the adsorbent; $[q]_t$ is the quantity of metal ions of charge n+ adsorbed at time t; $[q]_e$ is the quantity of metal ions of charge n+ adsorbed at equilibrium or infinity. A plot of ln(1 - F) against t gave a straight line (Fig 7b) and a higher R^2 value (Table 3) indicating a good fit of this model to the sorption process. The R^2 value of liquid film diffusion ($R^2 = 0.87$) being higher than that of intraparticle diffusion ($R^2 = 0.74$) suggests that adsorption process was surface diffusion dominant.
Both Bangham and Boyd models confirms that the kinetic was pseudo second-order diffusion and

adsorption mechanism governed by pore and surface diffusion. The mathematical expression of Bangham and Boyd models are given in Eq. 17 & 18 (Dada *et al.,* 2015a; Sun *et al.,* 2008; Bajpai and Rohit 2009):

$$\log\log\left(\frac{Co}{Co - q_t m}\right) = \log\left(\frac{k_o m}{2.303V}\right) + \alpha\log(t)$$

$$(17)$$

$$B_t = -0.4977 - \ln(1 - F) \qquad (18)$$

Considering the Boyd equation, B_t is the mathematical function of F and F is the fraction of adsorbate adsorbed at time t evaluated as:

$$F = \frac{q_t}{q_e} \qquad (19)$$

α and K_o from Bangham model are constants determined from slope and intercept of best line

ADEWUMI O DADA[1], DAYO F LATONA[2], OLUSEGUN J OJEDIRAN[3], OSAZUWA O. NATH [1]*

equation. Since the plot of $\log\log\left(\dfrac{Co}{Co-q_t m}\right)$

against $\log(t)$ gave a straight line (Fig 7c) with $R^2 =$ 0.8703 and α = 0.0108 (Table 3) value less than unity show that intraparticle diffusion or pore diffusion is one of the rate determining step.

However, the calculated B_t values were plotted against time t (Fig 7d). It was observed that the plot of B_t against t gave a straight line that does not pass through the origin with $R^2 = 0.88$ close to unity suggesting that both pore and surface diffusion played key roles in the adsorption process.
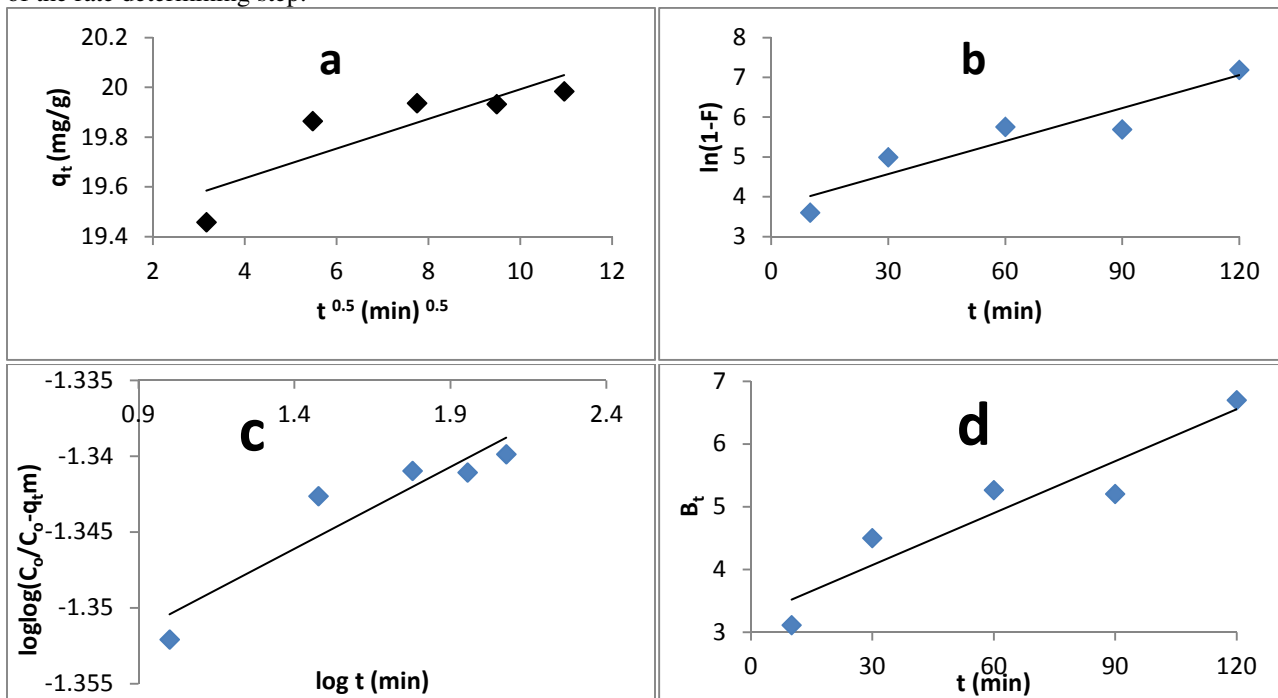
Figs 7. Linearized plots of (a) Intraparticle diffusion (b) liquid film diffusion (c) Bangham and (d) Boyd models of adsorption mechanism for sorption of Cu^{2+} onto BS-Mn nanocomposite

Table 3

Adsorption Mechanism models for immobilization of Cu^{2+} onto BS-Mn nanocomposite

Intraparticle Diffusion	Parameters	Liquid Film Diffusion	parameters	Bangham	Parameters	Boyd	parameter
$k_{id}(mg/g/min^{0.5})$	5.96 x10^{-2}	k_{fd}	0.0276	K_o	5x10^{-2}	R^2	0.8853
C	19.397			α	0.0108		

Adsorption Isotherm: Adsorption is usually modeled by isotherms which relate the relative concentration of solute adsorbed on to that of the solute in solution. The equilibrium sorption data were analyzed using five of the two-parameter isotherm models: Langmuir, Freundlich, Temkin, Dubinin-Kaganer-Raduskevich (DRK) and Flory-Huggins presented in Figs 8 (a – e) respectively.

Langmuir isotherm model is based on the assumption that monolayer adsorption takes place only at specific localized sites on the energetically homogeneous surface of adsorbent and the saturation coverage corresponds to complete occupancy of these sites; each site can accommodate one and only one adsorbate; there is no interaction between neighboring adsorbed molecules

neither are there phase transitions (Leszek *et al.,* 2000). The linearized Langmuir isotherm is given in Eq. 20:

$$\frac{Ce}{Q_e} = \frac{1}{K_L Q_{max}} + \frac{C_e}{Q_{max}} \qquad (20)$$

From the plot of C_e/Q_e against C_e (Fig 8a), and evaluated parameters in Table 4, $K_L = 2.191$, is Langmuir isotherm constant (L.mg^{-1}) related to the energy of adsorption. The essential feature of the Langmuir isotherm is expressed in terms of equilibrium parameter R_L, which is a dimensionless constant, referred to as separation factor (Prasad and Elumalai, 2011):

ADEWUMI O DADA[1]*, DAYO F LATONA[2], OLUSEGUN J OJEDIRAN[3], OSAZUWA O. NATH [1]

$$R_L = \frac{1}{1+K_L C_o} \qquad (21)$$

The value of R_L (Fig 8f) ranging from $4.53 \times 10^{-3} - 2.2 \times 10^{-2}$ which is less than unity is an indication of a favourably adsorption. The coefficient of correlation, $R^2 = 0.961$ suggests that equilibrium data were well described Langmuir isotherm model signifying that a chemisorption adsorption dominating (Hao *et al.*, 2010). The copper adsorption capacity (q_{max}) on BS-Mn at room temperature was 44.64 mgg^{-1}. This was much higher than adsorption capacity of other adsorbent reported in the literature for sorption of copper: Zerovalent iron nanoparticle (40.8.16) (Dada *et al.*, 2014); Chitosan-bound Fe_3O_4 magnetic nanoparticles (21.5 mgg^{-1}) (Ho *et al.*, 2005); Amino-functionalized magnetic nanosorbent (25.77 mgg^{-1}) (Hao *et al.*, 2010); Magnetic nano-adsorbent modified by gum Arabic (38.5 mgg^{-1}) (Banerjee and Chen 2007); Hydroxyapatite nanoparticles (36.9 mgg^{-1}) (Wang *et al.*, 2009) and Maghemite nanoparticle (27.7 mgg^{-1}) (Hu *et al.*, 2006).

Freundlich isotherm model relates to both monolayer (chemisorption) and multilayer (physisorption) adsorption whose expression encompasses the surface heterogeneity and the exponential distribution of active sites and their energies. The Linear form of Freundlich equation is given (Ahmad *et al.*, 2014b):

$$logQ_e = log K_f + \frac{1}{n} log C_e \qquad (19)$$

The Freundlich isotherm constants, K_f (27. 48 mgg^{-1}) and n (4.88) (Fig 8b, Table 4) indicating the sorption capacity and intensity respectively are parameters characteristic of the BS–Mn–Cu system determined from the intercept and slope of the linear plot of *Log Q_e* against *Log C_e*. Since the value of n lies between one and ten and 1/n being less than unity are reflections of favorable and normal adsorption respectively (Dada *et al.*, 2012). The R^2 value (0.9195) close to unity but less than that of Langmuir suggests that Langmuir isotherm model better represents equilibrium data

Temkin isotherm model gives more formation about the heat of adsorption which decreased as a result of surface coverage due to adsorbent – adsorbate interactions. Its linear equation is given in Eq. 20 (Dada *et al.*, 2013):

$$Q_e = B \ln A_T + B \ln Ce . \qquad (20)$$

B=RT/b_T, where b_T (Temkin isotherm constant) related to the heat of sorption and A_T is the Temkin isotherm equilibrium binding constant (Lg^{-1}) evaluated as 517.995

Jmol^{-1} and 597.588 *Lg^{-1}* respectively (Table 4). The values of these constants were determined from the slope and intercept obtained from best fit plot of Q_e versus *lnCe* (Fig 8c) with a good correlation coefficient ($R^2 = 0.9042$).

Dubinin-Kaganer-Raduskevich (DKR) isotherm curve is related to porous structure of the BS-Mn. The linear equation of this isotherm model is given as (Kordosky 2002):

$$\ell n Q_e = \ell n Q_d - D_{DKR}\, \varepsilon^2 \qquad (21)$$

The parameter ε is the Polanyi potential which is computed as (Foo and Hameed, 2010):

$$\varepsilon = RT\ell n\left[1+\frac{1}{C_e}\right] \qquad (22)$$

Where Q_d is the theoretical isotherm saturation capacity (mg/g), D_{DKR} is the DKR isotherm constant (mol^2/kJ^2) related to free adsorption energy. The values of Q_d (36.833 mg g^{-1}) and D_{DKR} (1×10^{-8}) presented in Table 4 were determined respectively from the slope and intercept of the plot of *ln Qe versus* ε^2. This model was applied to distinguish the physical and chemical adsorption of metal ions with its mean free energy, E per molecule of adsorbate given as (Ho *et al.*, 2002):

$$E = -\left[\frac{1}{\sqrt{2D_{DKR}}}\right] \qquad (23)$$

From the plot Fig. 8d and evaluated parameters in Table 4, it was observed that the equilibrium data fitted also to DKR model based on the $R^2 \approx 0.93$ better. It can therefore be suggested that E value greater than 7 kJ mol^{-1} was an indication of chemical nature of the adsorption mechanism.

Flory –Huggins Isotherm Model is generally used to account for the surface coverage of the adsorbate on the adsorbent. Its linear expression is given in Eq. 24 below (Foo and Hameed 2010; Febrianto *et al.,* 2009):

$$Log\left(\frac{\theta}{C_o}\right) = LogK_{FH} + n_{FH}Log(1-\theta) \qquad (24)$$

Where $\theta = 1 - \left(\frac{Ce}{C_o}\right) \qquad (25)$

θ is the degree of surface coverage, n_{FH} *and* K_{FH} are Florry-Huggin's constants related to number of metal

ADEWUMI O DADA[1]*, DAYO F LATONA[2], OLUSEGUN J OJEDIRAN[3], OSAZUWA O. NATH [1]

ions remaining on the adsorption sites and the equilibrium constant of adsorption respectively determined from the linear plot of $Log(\theta/C_o)$ versus log

$(1 - \theta)$ (Fig 8e). Positive value of K_{FH} (0.1019) is an indication of a feasible and spontaneous adsorption.
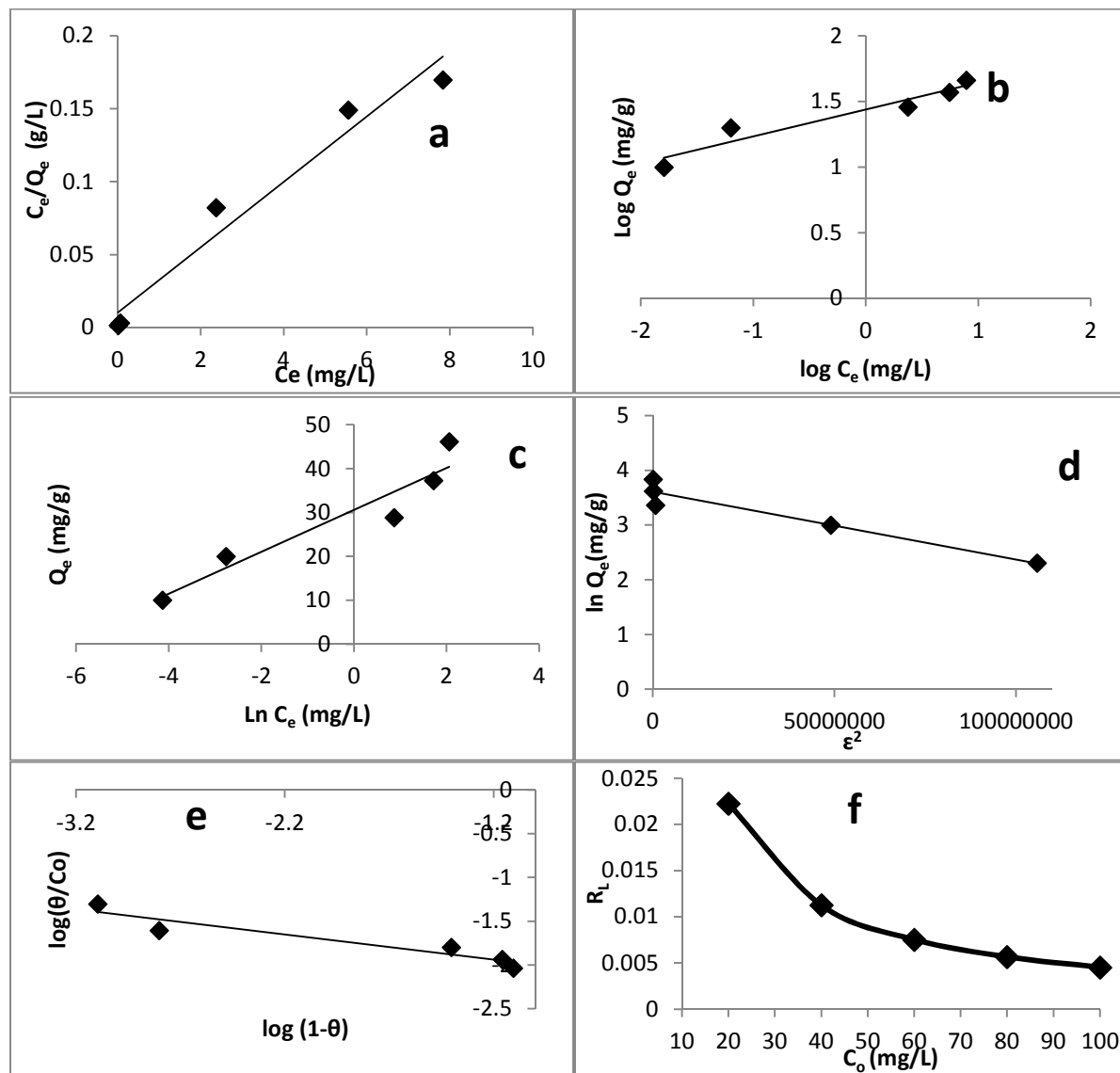

Fig. 8 Linearized plots of (a) Langmuir (b) Freundlich (c) Temkin (d) D-R and (e) Flory-Huggins Isotherm model for adsorption of Cu^{2+} onto BS-Mn Nanocomposite and (f) Langmuir separation factor

Table 4: Isotherm models constants' for the sorption of Cu^{2+} onto BS – Mn Nanocomposite

Langmuir		Freundlich		Temkin		DRK		Flory-Huggins	
$q_{max}\,(mgg^{-1})$	44.643	k_f	27.4853	$b_T\,(Jmol^{-1})$	517.995	q_d	36.833	K_{FH}	0.1019
$K_L\,(Lmg^{-1})$	2.1961	$1/n$	0.2049	$\beta(Lg^{-1})$	30.583	D_{DRK}	1×10^{-8}	n_{FH}	-0.2871
R_L	4.53×10^{-3} - 2.2×10^{-2}	n	4.8804	$A_T(Lg^{-1})$	597.588	E(kJ/mol)	7.071		
R^2	0.9611	R^2	0.9195	R^2	0.9042	R^2	0.9261	R^2	0.8929

Thermodynamic Studies: In order to further determine whether the adsorption of copper (II) ions onto BS-Mn nanocomposite will occur spontaneously, thermodynamic parameters were significant process for the practical application of this adsorbent. Effect of

temperature is highly imperative in every transfer phenomenon such as adsorption because some thermodynamics parameters such as enthalpy change (ΔH^o), entropy change (ΔS^o) and Gibbs free energy change (ΔG^o) could be determined. Fig. 9 shows the

ADEWUMI O DADA[1]*, DAYO F LATONA[2], OLUSEGUN J OJEDIRAN[3], OSAZUWA O. NATH [1]

effect of temperature on the adsorption of Cu^{2+} onto BS-Mn at 298 K, 308 K, 323 K and 338 K. It was observed that increase in temperature led to increase in the removal efficiency of Cu^{2+} which was due to increase in number of active sites and the decrease in the thickness of the boundary layer surrounding the adsorbent. 99.8% removal efficiency (Fig 9) was attained at 323 K supporting the findings of Dada *et al.,* (2015a); Doğan *et al.,* (2009). Moreover, increasing temperature resulted in an increase in the rate of approach to equilibrium suggesting that the adsorption process would be endothermic in nature.

The data obtained from the effect of temperature were analyzed using the Van't Hoff's equation (Ayanda *et al.,* 2013; Boparai *et al.,* 2011):

$$LogK_C = \frac{\Delta S}{2.303R} - \frac{\Delta H}{2.303RT} \qquad (27)$$

The Van't Hoff plot of Log Kc versus 1/T (Fig 10) gave a straight line with a best fit with coefficient of correlation close to unity ($R^2 = 0.97$) (Table 5). The thermodynamics parameters, standard enthalpy change ΔH^o (kJ mol^{-1}) and standard entropy change ΔS^o (J $mol^{-1}K^{-1}$) were determined from the slope and intercept of Eq. (27) respectively. The standard Gibbs free energy ΔG^o (kJ mol^{-1}), was calculated using Eq. 28:

$$\Delta G = -2.303RT \ell ogKc \qquad (28)$$

From the calculated thermodynamic parameters for the adsorption of copper (II) ions (Table 5), the enthalpy change value obtained was positive indicating confirming that the adsorption of copper (II) ions onto BS-Mn was endothermic. The evaluated standard Gibbs free energy ΔG^o values were negative indicating that the adsorption was spontaneous and feasible and the value of standard entropy change ΔS^o suggested increase in

randomness of the process at the solid/liquid interface during adsorption of the copper (II) ions onto BS–Mn (Dada *et al.,* 2015a; Edward *et al.,* 2008; Hao *et al.,* 2010; Jinxuan *et al.,* 2012)
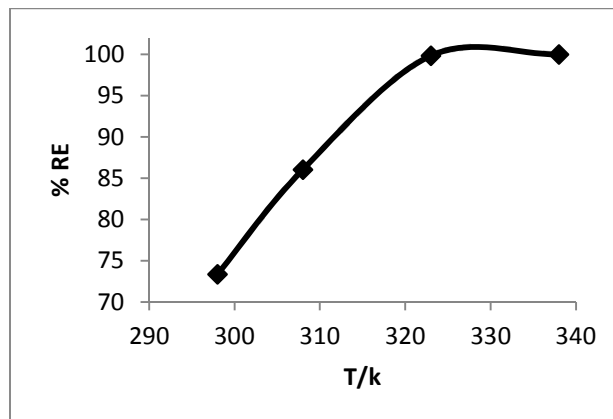

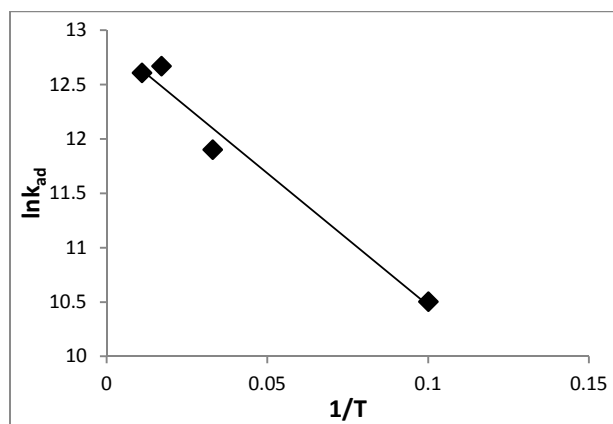**Fig 9**: The effect of Temperature on Cu^{2+} adsorbed onto BS–Mn

Fig 10: Van't Hoff plot on sorption of Cu^{2+} adsorbed onto BS–Mn

Table 5: Thermodynamic parameters for adsorption of Cu^{2+} onto BS-Mn

Nano-adsorbent	T/K	ΔG (kJmol^{-1})	ΔH (kJmol^{-1})	ΔS (Jmol^{-1}K^{-1})	R^2	lnK$_c$
BS–Mn	298	-31.773	202	107.3	0.975	12.982
	308	-32.846				12.979
	323	-34.456				12.975
	338	-36.065				12.971

Conclusion: Bamboo supported manganese nanocomposite (BS-Mn) was successfully prepared in a single pot system via bottom-up using chemical reduction approach. This study revealed that adsorption of Cu^{2+} onto BS-Mn nanocomposite depended on various operational parameters such as: effects of initial concentration, contact time, pH, adsorbent dose and temperature. Kinetics data were best described by pseudo second-order as validated by statistical tools. The mechanism was chemisorption and was pore diffusion dominated confirmed. The equilibrium sorption data showed a better by the Lngmuir isotherm hence, signifying the applicability of monolayer coverage of copper on BS-Mn surface. Outcome of the

ADEWUMI O DADA[1]*, DAYO F LATONA[2], OLUSEGUN J OJEDIRAN[3], OSAZUWA O. NATH [1]

thermodynamic studies revealed that adsorption was feasible, spontaneous and endothermic in nature. BS-Mn is therefore recommended as an effective and potential nanocomposite for heavy metal scavenger from wastewater.

*Acknowledgment***:** Dada, A.O and co-authors appreciate the management of Landmark University for facilities, opportunity and serene environment granted to carry out result oriented research.

REFERENCES

Adekola, FA; Abdus-Salam, N; Adegoke, HI; Adesola, AM; Adekeye, JID (2012) Removal of Pb(II) from aqueous solution by natural and synthetic calcites. *Bull. Chem. Soc. Ethiop*. 26(2): 195-210.

Ahmad, MA; Puad, NAA; Bello, OS (2014)[a]. Kinetic, equilibrium and thermodynamic studies of synthetic dye removal using pomegranate peel activated carbon prepared by microwave-induced KOH activation. *Water Resources and Industry*, 6: 18 – 35.

Ahmad, MA; Ahmad, N; Bello, OS (2014)[b] Adsorptive Removal of Malachite Green Dye Using Durian Seed-Based Activated Carbon. *Water Air Soil Pollut*, 225: 2057 [(a)]. Doi 10.1007/s11270-014-2057-z

Ayanda, OS; Fatoki, SO; Adekola, FA; Ximba, BJ (2013). Kinetics and equilibrium models of the sorption of tributyltin to nZnO, activated carbon and nZnO/activated carbon composite in artificial seawater. *Marine and Pollution Bulletin*, 72(1) (2013) 222- 230.

Azizian, NS. (2004) Kinetic models of sorption: a theoretical analysis, J. Colloid Interface Sci. 276: 47–52.

Bajpai, SK; Rohit VK (2009) Removal of hexavalent chromium from aqueous solutions by Sorption into a Novel Sawdust Anion Exchanger (SAE) Sorbent. *J Environl Prot Sci*, 3: 23 – 33.

Banerjee, SS; Chen, D.H. (2007). Fast removal of copper ions by gum Arabic modified magnetic nano-adsorbent, *J. Hazard. Mater.* 147: 792–799

Bonnie, RS; Marc, S; Daniel, K; Peter, A; Tar-Ching SB. (2007). Copper And Human Health: Biochemistry, Genetics, And Strategies For Modeling Dose-Response Relationships" *Journal of Toxicology and Environmental Health*, Part B, 10: 157–222,

Boparai, HK; Meera, J; Dennis, MO (2011). Kinetics and thermodynamics of Cadmium ion removal by adsorption onto nano-zerovalent iron particles. *Journal of Harzardous Material,* 186 (1): 458 – 465

Chingombe, P; Saha, B; Wakeman, RJ (2006). Sorption of atrazine on conventional and surface modified activated carbons, *J. Colloid Interface Sci.*, 302: 408–416.

Dada, AO; Adekola, FA; Odebunmi, EO (2015)[a] Kinetics and equilibrium models for Sorption of Cu(II) onto a Novel Manganese Nano-adsorbent. *Journal of Dispersion Science and Technology* 37(1): 119 – 133

Dada, AO; Adekola, FA; Odebunmi, EO (2015)[b]. A novel zerovalent manganese for removal of copper ions: synthesis, characterization and adsorption studies. Applied Water Science (Springer). Doi: 10.1007/s13201-015-0360-5

Dada, AO; Olalekan, AP; Olatunya, AM; Dada, O (2012). Langmuir, Freundlich, Temkin and Dubinin–Radushkevich Isotherms Studies of Equilibrium Sorption of Zn^{2+} unto Phosphoric Acid Modified Rice Husk. *Journal of Applied Chemistry*, 3(2): 38-45

Dada, AO; Ojediran, JO; Olalekan, AP (2013).Sorption of Pb^{2+} from Aqueous Solution unto Modified Rice Husk: Isotherms Studies. Advances in Physical Chemistry.2013, http://dx.doi.org/10.1155 /2013/842425

Dada, AO; Adekola, FA; Odebunmi, EO (2014). Isotherm, kinetics and thermodynamics studies of sorption of Cu^{2+} onto novel zerovalent iron nanoparticles. *Covenant Journal of Physical and Life Sciences*, 2(1), 24 – 53.

Dhermendra, K; Tiwari, BJ; Prasenjit, S (2008). Application of Nanoparticles in Waste Water Treatment" *World Applied Sciences Journal*, 3(3): 417 – 433

Doğan, M; Türkyilmaz, A; Alkan, M; Demirbaş, Ö (2009). Adsorption of copper (II) ions onto sepiolite and electrokinetic properties. Desalin **238**: 257–270

Edward, LK; Mui, WH; Cheung, V; Lee, KC; Gordon, M (2008).Kinetic Study on Bamboo Pyrolysis, *Ind. Eng.Chem. Res.* 47: 5710–5722.

ADEWUMI O DADA[1]*, DAYO F LATONA[2], OLUSEGUN J OJEDIRAN[3], OSAZUWA O. NATH [1]

Fawell, JK; Ohania, (2004). Copper in Drinking Water" WHO Guidelines for Drinking-water Quality, *Fax: +4122791 4806; e-mail: permissions@who.int*

Febrianto, J; Kosasih, AN; Sunarso, J; Ju, Y-H; Indraswatib, N; Ismadji, S (2009). Equilibrium and kinetic studies in adsorption of heavy metals using biosorbent: A summary of recent studies, J Hazard Mater. 162: 616–645

Foo, KY; Hameed BH (2010) Review: Insights into the modeling of adsorption isotherm systems. *Chem Engg J.* 156: 2 – 10.

Fu-Lan, H; Yu-Chen, P; Hong-L, L (2009). Removal of Heavy Metal Ions from Aqueous Solutions by Bamboo Wastes. *Taiwan J For Sci.*.24 (3): 159-68

Hameed, BH; Mahmoud, DK; Ahmad, AL (2008). Equilibrium modeling and kinetic studies on the adsorption of basic dye by a low-cost adsorbent: Coconut (Cocos nucifera) bunch waste, J Hazard Maters., 158: 65–72

Hao, Y-M; Chen, M; Hu, Z-B. (2010) Effective removal of Cu (II) ions from aqueous solution by amino-functionalized magnetic nanoparticles, J Hazard Maters. 184: 392–399

Ho, Y.S. (2004). Citation review of Lagergren kinetic rate equation on adsorption reactions, *Scientometrics* 59 171–177.

Ho, YS; Porter, JF; Mckay, G (2002). Equilibrium Isotherm studies for the sorption of divalent metal ions onto peat: Copper, Nickel and Lead single component systems. Water, Air and Soil Pollution, 141: 1 – 33.

Ho, Y-S; Chiang, T-H; Hsueh, Y-M (2005). Removal of basic dye from aqueous solution using tree fern as a biosorbent, Process Biochemistry, 40: 119–124

Hsu, F-L; Peng, Y-C; Lee, H-L (2009). Removal of Heavy Metal Ions from Aqueous Solutions by Bamboo Wastes. *Taiwan J For Sci* 24(3): 159-1 68

Hu, J; Chen, GH; Lo, IMC (2006). Selective removal of heavy metals from industrial wastewater using maghemite nanoparticle: Performance and mechanisms, J. Environ. Eng.—ASCE, 132: 709–715.

Igwe, J C; Abia, AA (2006). A bioseparation process for removing heavy metals from waste water using biosorbents. *African J. Biotech.* 5 (12): 1167-1179.

Igwe, JC; Abia, AA; Ibeh, CA (2008). Adsorption kinetics and intraparticulate diffusivities of Hg, As and Pb ions on unmodified and thiolated coconut fiber. Int. J. Environ. Sci. Technol. 5, 83–92.

Jinxuan, H; Heather, J; shepley (2012) "Evaluation of desorption of Pd(II), Cu(II) and Zn(II) form titanium dioxide nanoparticles, *Science of the Environment*, 331: 209 – 220

Jun, MA; Nancy, MB (2000). Zinc and copper intake and major food sources for older adult in the 1994-96 continuing survey of food intakes b individual. *Journal Nutr*, 130 (11): 2838 – 2843

Kordosky, AG (2002). Copper recovery using leach/solvent extraction and electrowinning technology: Forty years of innovation, 2.2 million tonnes of copper annually. *Journal of the South African Institute of Mining and Metallurgy*, SA, pp 445 – 450

Leszek, C; Mieczyslaw, RB; Ewa, K-C (2000). Some generalization of Langmuir adsorption isotherm,'' University of Mining and Metallurgy, Faculty of Fuels and Energy, al. Mickiewicza 30, 30-059 Cracow, Poland.

Lo, S-F; Wang, S-Y; Tsai, M-J; Lin, L-D (2012). Adsorption capacity and removal efficiency of heavy metal ions by Moso and Ma bamboo activated carbons. *Chemical Engineering Research and Design* 90, 1397–1406

Michael, SP; John, JC; Gary, AP (2001). *Aspergillus niger* absorbs copper and zinc from swine wastewater" *Bioresource Technology*, 77: 41 – 49

Nuran, E; Hande, GO; Nukhet, AB (2000). Toxic metals and oxidative stress, mechanism involved in metal induced oxidative damage, *Medical chemistry,* 1 (6): 529 – 539

Ozcan, A; Ozcan, AS; Gok, O (2007). Adsorption kinetics and isotherms of anionic dye of reactive blue 19 from aqueous solutions onto DTMA-sepiolite, in: A.A. Lewinsky (Ed.), Hazardous Materials and Wastewater—Treatment, Removal and Analysis, Nova Science Publishers, New York, 2007.

Prasad, TNVKV; Elumalai, EK (2011). Biofabrication of Ag nanoparticles using moringa oleifera leaf extract and their antimicrobial activity. Asian Pacific Journal of Tropical Biomedicine Asian Pac

ADEWUMI O DADA[1]*, DAYO F LATONA[2], OLUSEGUN J OJEDIRAN[3], OSAZUWA O. NATH [1]

J Trop Biomed. **1**(6): 439–442. doi: 10.1016/S2221-1691(11) 60096-8

Srivastava, VC; Mall, ID; Mishra, IM (2006). Characterization of mesoporous rice husk ash (RHA) and adsorption kinetics of metal ions from aqueous solution onto RHA. *Journal of Hazardous Material*, 134 (1-3), 257 –267

Song, C; Wu, S; Cheng, M; Tao, P; Shao, M; Gao, G (2014). Adsorption Studies of Coconut Shell Carbons repared by KOH Activation for Removal of Lead (II) from Aqueous Solutions. *Sustainability*, 6: 86-98.

Sun, X-F; Wang, S-G; Liu, X-W; Gong, W-X; Bao, N; Gao, B-Y; Zhang, H-Y (2008). Biosorption of Malachite Green from aqueous solutions onto aerobic granules: Kinetic and equilibrium studies. *Bioresource Technology* **99**: 3475–3483

Wang, YJ; Chen, JH; Cui, YX; Wang, SQ; Zhou, DM (2009). Effects of low-molecularweight organic acids on Cu(II) adsorption onto hydroxyapatite nanoparticles, *J. Hazard. Mater*.162: 1135–1140.

Weber, WJ; Morris, JC (1963). Kinetics of Adsorption on Carbon from Solution", J. Sanit. Eng. Div. ASCE, 89: 31-59. Mater. **161**: 848–853

Wu, FC; Tseng, RL; Juang, RS (2009). Initial behavior of intraparticle diffusion model used in the description of adsorption kinetics, *Chem. Eng. J.* 153: 1–8.

Xiao, S; Ma, H; Shen, M; Wang, S; Huang, Q; Shi, X (2011). Excellent copper (II) removal using iron nanoparticle-immobilized hybrid electrospun polymer nanofibrous mats. *Colloid and Surface A: Physicochem. Eng. Aspects* 381: 48 – 54

Zhao, X-T; Zeng, T; Li, X-Y; Hu, ZJ; Gao, H-W; Xie, Z (2012). Modeling and Mechanism of the adsorption of copper ion onto natural bamboo sawdust. *Carbohydrate Polymers*, 89: 185– 192

ADEWUMI O DADA[1], DAYO F LATONA[2], OLUSEGUN J OJEDIRAN[3], OSAZUWA O. NATH [1]*